Inorg. Chem. **2005**, *44*, 2920–2925

A Ladderlike Chain Aluminum Fluoride $([Al_2F_8]^{2-})_n$ with Edge-Sharing AlF_6 Octahedra

Thierry Loiseau,*,† Hervé Muguerra,† Jerôme Marrot,† Gérard Férey,†,‡ Mohamed Haouas,† and Francis Taulelle†

Institut Lavoisier (UMR CNRS 8637) and Institut Universitaire de France, Université de Versailles St Quentin en Yvelines, 45, Avenue des Etats Unis, 78035 Versailles, France

Received November 3, 2004

A new aluminum fluoride, $Al_2F_8{\cdot}2NC_5H_6{\cdot}C_6H_3(CO_2H)_3$, was synthesized under mild hydrothermal conditions (200 °C, 3 days) in the presence of 1,3,5-benzenetricarboxylic acid (btc) in pyridine/HF (pyr/HF) solvent. Its structure is characterized with single-crystal XRD analysis and high-resolution solid-state NMR. The inorganic framework consists of the corner- and edge-shared connections of AlF_6 octahedra. They are linked via a common edge and form a bioctahedral motif which is trans-connected through the corner-shared fluorine. It results in the formation of an original infinite double file of AlF_6 octahedra running along the *a* axis. A high-power decoupled MAS $^{27}Al\{^{19}F\}$ Hahn echo NMR spectrum allowed us to distinguish the two crystallographic hexacoordinated Al sites. Four unresolved ^{19}F NMR signals are observed in the MAS spectra to account for the eight crystallographic fluorine atoms. Half of the terminal fluorine sites interact via strong hydrogen bonds with the ammonium groups of the pyridine moieties. The resulting mixed pyridine-fluoroaluminate chains are intercalated by the btc molecules which are hydrogen-bonded to the remaining free terminal fluoride anions through the protonated carboxylic acid function. The ^1H nuclei of both organic molecules are observed in the protonated form.

Introduction

There is a significant interest in the preparation of metal fluorides driven by the possibility of the formation of various inorganic networks.[1,2] For the past decade, organic molecules such as quaternary ammonium or protonated N-containing base cations were also used as counterions replacing the alkali or earth-alkali metals.[3] This has resulted in the formation of a wide variety of structures based on hydrogen bond interactions between the organic moieties and metal fluoride species. In this context, special attention has been paid to the synthesis of aluminum fluorides because the aluminum fluoride, AlF_3, material exhibits catalytic properties for industrial applications (ozone-friendly alternatives for chlorofluorocarbons[4−6]). The AlF_3 solid occurs in different polymorphs (α,[7] β,[8] γ,[9] *t*,[10] ϵ_2,[11] etc.), and some of them are obtained from the thermal decomposition of aluminum fluoride organic salts. For instance, the thermolysis of $[(CH_3)_4N][AlF_4]{\cdot}H_2O$ under vacuum at 450 °C produced the *t*-AlF_3[10] form. The nature of the mixed organic aluminum fluoride has a significant role since the specific AlF_3 form is prepared from one type of $R^+[AlF_n]^-$ precursor (R^+ = tetraalkylammonium or protonated amine). Thus, the reactivity of various organic molecules was intensively investigated in the aluminum−fluorine system. The result was the identification of a large number of organically templated fluoroaluminate phases with different dimensionalities. Most of them consist of isolated octahedral $[AlF_6]$ clusters surrounded by the organic species.[12−19] In other compounds,

* To whom correspondence should be addressed. E-mail: loiseau@chimie.uvsq.fr. Phone: 33 1 39 254 373. Fax: 33 1 39 254 358.
† Institut Lavoisier.
‡ Institut Universitaire de France.

(1) Massa, W.; Babel, D. *Chem. Rev.* **1988**, *88*, 275.
(2) Férey, G. *Encycl. Inorg. Chem.* **1994**, *3*, 1207.
(3) Bentrup, U.; Feist, M.; Kemnitz, E. *Prog. Solid State Chem.* **1999**, *27*, 75.
(4) Herron, N.; Thorn, D. L.; Harlow, R. L.; Davidson, F. *Chem. Mater.* **1995**, *7*, 75.
(5) Herron, N.; Farneth, W. *Adv. Mater.* **1996**, *8*, 959.
(6) Kemnitz, E.; Kohne, A.; Lieske, E. *J. Fluorine Chem.* **1997**, *81*, 197.
(7) Hoppe, R.; Kissel, D. *J. Fluorine Chem.* **1984**, *24*, 327.
(8) Le Bail, A.; Jacoboni, C.; Leblanc, M.; De Pape, R.; Duroy, H.; Fourquet, J.-L. *J. Solid State Chem.* **1988**, *77*, 96.
(9) Shinn, D. B.; Crocket, D. S.; Haendler, H. M. *Inorg. Chem.* **1966**, *5*, 1927.
(10) Le Bail, A.; Fourquet, J.-L.; Bentrup, U. *J. Solid State Chem.* **1992**, *100*, 151.
(11) Alonzo, C.; Morato, A.; Medina, F.; Guirado, F.; Cesteros, Y.; Salagre, P.; Sueiras, J. E.; Terrado, R.; Giralt, A. *Chem. Mater.* **2000**, *12*, 1148.
(12) Mitteilung, K.; Bukovec, P. *Monatsh. Chem.* **1983**, *114*, 277.

10.1021/ic048461z CCC: $30.25
Published on Web 03/11/2005

larger isolated species ($[Al_3F_{12}]$,[20] $[Al_4F_{20}]$,[21] and $[Al_7F_{30}]$[22]) or the oxo-fluorinated ϵ-Keggin cation Al_{13}[23,24] was reported, and the chainlike structures of corner-shared $[AlF_6]$ units were also encountered.[22,25−27] In a few rare cases, edge-shared bioctahedral $[Al_2F_8]$ motifs have been isolated in molecular,[28−30] chainlike[31] (in this phase, an isolated tetrahedral $[AlF_4]$ was also observed), or layered[32] structures.

In this contribution, we report on a new form of chainlike aluminum fluoride $Al_2F_8{\cdot}2NC_5H_6{\cdot}C_6H_3(CO_2H)_3$ hydrothermally synthesized in the presence of 1,3,5-benzenetricarboxylic acid (btc) and a solution of pyridine/HF (pyr/HF) as solvent. This work was a part of our systematic study of the reactivity of aluminum with carboxylic acids containing benzene rings.[33,34] This phase exhibits a very original connection mode for the AlF_6 octahedra consisting of the linkage of an edge-shared bioctahedral unit via the fluorine corner to generate an infinite double chain running along the *a* axis. In this solid, three configurations for the Al−F bonds occur; they are terminal, bridging, and edge sharing. This unique feature was characterized by means of single-crystal XRD analysis and multinuclear solid-state NMR (^{27}Al, ^{19}F, and ^{1}H).

Experimental Section

Synthesis. The aluminum fluoride $Al_2F_8{\cdot}2NC_5H_6{\cdot}C_6H_3(CO_2H)_3$ was hydrothermally synthesized in the presence of btc under autogenous pressure with a solution of pyr/HF as the solvent. The starting reactants were aluminum nitrate ($Al(NO_3)_3{\cdot}9H_2O$, Carlo Erba Regenti, 98%), pyr/HF (C_5H_5N/HF, Aldrich, 30:70%), and btc ($C_6H_3(CO_2H)_3$, Aldrich, 95%). Typically, the reaction mixture containing Al (1.314 g), btc (0.3677 g), and pyr/HF (5 mL) in a 2:1:29 molar ratio was placed in a 23 mL Teflon-lined steel Parr autoclave at 200 °C for 3 days. The synthesis pH was 1. A white powdered product was filtered, washed with deionized water, and dried in air at room temperature. Optical microscope analysis indicated that the sample is composed of flat needlelike crystals 200−500 μm in size. The preliminary X-ray powder diffraction pattern showed it to be a novel phase.

Elemental analysis (CNRS Analysis Center, Vernaison, France). Al: obs, 8.64%; calc, 9.4%. F: obs, 26.37%; calc, 26.4%.

Table 1. Crystal Data and Structure Refinement for $Al_2F_8{\cdot}2NC_5H_6{\cdot}C_6H_3(CO_2H)_3$

empirical formula	$Al_2F_8N_2O_6C_{19}H_{18}$
formula weight	576.31
temperature	298(2) K
wavelength	0.71073 Å
crystal system, space group	triclinic, $P\bar{1}$
unit cell dimensions	$a = 7.2192(2)$ Å, $\alpha = 81.230(2)°$ $b = 8.8443(3)$ Å, $\beta = 84.417(2)°$ $c = 17.2514(6)$ Å, $\gamma = 89.450(2)°$
volume	1083.42(6) Å^3
Z, calculated density	2, 1.767 Mg m^{-3}
absorption coefficient	0.246 mm^{-1}
final R indices [$I > 2\sigma(I)$]	R1[a] = 0.0362, wR2[b] = 0.0977
R indices (all data)	R1[a] = 0.0516, wR2[b] = 0.1128

[a] $R1 = \sum||F_o| - |F_c||/\sum|F_o|$. [b] $wR2 = \{\sum[w(|F_o|^2 - |F_c|^2)^2]/\sum[w(|F_o|^2)^2]\}^{1/2}$ and $w = 1/[\sigma^2(F_o^2) + (0.0707P)^2]$ where $P = [(F_o^2) + 2F_c^2]/3$.

Single-Crystal X-ray Structure Analysis. A colorless needle-shaped crystal (0.30 × 0.04 × 0.01 mm) was selected with a polarizing optical microscope and glued onto a glass fiber for a single-crystal X-ray diffraction experiment. X-ray intensity data were collected on a Bruker X8-APEX2 CCD area-detector diffractometer using Mo Kα radiation (λ = 0.71073 Å). Four sets of narrow data frames (60 s per frame) were collected at different values of θ with initial values for both ϕ and ω of 2 and 0.3° increments of ϕ or ω. Data reduction was accomplished using SAINT V7.03. The substantial redundancy of the data allowed a semiempirical absorption correction (SADABS V2 × 10[35]) to be applied on the basis of multiple measurements of equivalent reflections. The structure was solved by direct methods, developed by successive difference Fourier syntheses, and refined by full-matrix least-squares on all F^2 data using SHELXTL V6.12.[36] Hydrogen atoms were included in calculated positions and allowed to ride on their parent atoms. The structure was solved in space group $P\bar{1}$ using the direct methods. The two unique aluminum and eight fluorine atoms were first revealed, and the remaining atoms (O, C, and N) were placed by successive Fourier map analyses. The hydrogen atoms were placed using geometrical constraints. This also includes the additional hydrogen atoms bonded to the nitrogen atoms of the pyridine molecule which was protonated once to balance the negative charge of the fluoroaluminate species. The final refinement including anisotropic thermal parameters of all non-hydrogen atoms converged to R1 = 0.0362 and wR2 = 0.0977. All the calculations were performed by using the SHELX-TL program on the basis of F^2. The crystal data are given in Table 1.

IR Spectroscopy. The IR spectrum was recorded on a Nicolet 550 FTIR spectrometer at room temperature in the 400−2000 cm^{-1} range using a potassium bromide pellet. The IR spectrum of $Al_2F_8{\cdot}2NC_5H_6{\cdot}C_6H_3(CO_2H)_3$ shows the vibrational bands in the usual

(13) Bentrup, U.; Ahmadi, A.; Kang, H.-C.; Massa, W. *Z. Anorg. Allg. Chem.* **1998**, *624*, 1465.
(14) Rother, G.; Worzala, H.; Bentrup, U. *Z. Kristallogr.−New Cryst. Struct.* **1998**, *213*, 119.
(15) Goreshnik, E.; Leblanc, M.; Maisonneuve, V. *Acta Crystallogr. E* **2003**, *59*, m1059.
(16) Schröder, L.; Frenzen, G.; Massa, W. *Z. Anorg. Allg. Chem.* **1993**, *619*, 1307.
(17) Rother, G.; Worzala, H.; Bentrup, U. *Z. Anorg. Allg. Chem.* **1996**, *622*, 1991.
(18) Touret, J.; Bourdon, X.; Leblanc, M.; Retoux, R.; Renaudin, J.; Maisonneuve, V. *J. Fluorine Chem.* **2001**, *110*, 133.
(19) Adil, K.; Goreshnik, E.; Courant, S.; Dujardin, G.; Leblanc, M.; Maisonneuve, V. *Solid State Sci.* **2004**, *6*, 1229.
(20) Tang, L.-Q.; Dadachov, M. S.; Zou, X.-D. *Z. Kristallogr.−New Cryst. Struct.* **2001**, *216*, 385.
(21) Domesle, R.; Hoppe, R. *Angew. Chem., Int. Ed. Engl.* **1980**, *19*, 489.
(22) Goreshnik, E.; Leblanc, M.; Maisonneuve, V. *Z. Anorg. Allg. Chem.* **2002**, *628*, 162.
(23) Yu, P.; Lee, A. P.; Phillips, B. L.; Casey, W. H. *Geochim. Cosmochim. Acta* **2003**, *67*, 1065.
(24) Allouche, L.; Taulelle, F. *Chem. Commun.* **2003**, 2084.
(25) Phan Thanh, S.; Renaudin, J.; Maisonneuve, V. *Solid State Sci.* **2000**, *2*, 143.
(26) Phan Thanh, S.; Gaslain, F.; Leblanc, M.; Maisonneuve, V. *J. Fluorine Chem.* **2000**, *101*, 161.
(27) Goreshnik, E.; Leblanc, M.; Gaudin, E.; Taulelle, F.; Maisonneuve, V. *Solid State Sci.* **2002**, *4*, 1213.
(28) Herron, N.; Harlow, R. L.; Thorn, D. L. *Inorg. Chem.* **1993**, *32*, 2985.
(29) Adamczyk, B.; Troyanov, S. I.; Schneider, M.; Kemnitz, E. *Z. Anorg. Allg. Chem.* **2000**, *626*, 2543.
(30) Tang, L.-Q.; Dadachov, M. S.; Zou, X.-D. *Z. Kristallogr.−New Cryst. Struct.* **2001**, *216*, 389.
(31) Herron, N.; Thorn, D. L.; Harlow, R. L.; Davidson, F. *J. Am. Chem. Soc.* **1993**, *115*, 3028.
(32) Harlow, R. L.; Herron, N.; Li, Z.; Vogt, T.; Solovyov, L.; Kirik, S. *Chem. Mater.* **1999**, *11*, 2562.
(33) Loiseau, T.; Serre, C.; Huguenard, C.; Fink, G.; Taulelle, F.; Henry, M.; Bataille, T.; Férey, G. *Chem.—Eur. J.* **2004**, *10*, 1373.
(34) Loiseau, T.; Mellot-Draznieks, C.; Muguerra, H.; Férey, G.; Haouas, M.; Taulelle, F. *C. R. Chim.* **2005**, in press.
(35) *APEX2*, version 1.0−8; Bruker AXS: Madison, WI, 2003.
(36) *SHELXTL*, version 6.12; Bruker AXS: Madison, WI, 2001.

range (1400−1750 cm^{-1}) for the carboxylic function. Strong absorption bands located at 1735 and 1685 cm^{-1} are assigned to C−OH, indicating that the btc species is present with its protonated form (−CO_2H).

Thermogravimetric Analysis. The thermogravimetric analysis (under N_2, 3 °C min^{-1}, TA Instrument 2050) shows that the title compound starts to decompose at 210 °C and a continuous weight loss is observed up to 750 °C. It is assigned to the departure of pyridine and trimesic acid molecules. At 800 °C, the XRD pattern of the residue corresponds to that of the aluminum fluoride α-AlF_3.[7]

Solid-State NMR. All spectra were collected with a Bruker Avance 500 spectrometer using a 2.5 mm triple resonance ($^1H/^{19}F-X$) MAS probe. Powder samples were packed into 2.5 mm ZrO_2 rotors. Measurements were carried out at room temperature. ^{27}Al (130.3 MHz) and ^{19}F (470.5 MHz) spectra were referenced to external alum ($(NH)_4Al(SO_4)_2 \cdot 12H_2O$) at −0.6 ppm relative to 1 M aqueous $Al(NO_3)_3$ and to NaF at −221 ppm relative to $CFCl_3$, respectively. ^1H (500.1 MHz) data were referenced to standard tetramethylsilane (TMS) using adamantane signals at 1.7 ppm. The ^1H spectrum was collected with single-pulse acquisition at a spinning rate of 30 kHz using 5 μs pulses, which correspond to $\pi/4$ excitation angle, and 2.6 W power. To suppress the strong background signal from the probe head, ^{19}F data were collected using the Hahn echo sequence with 5.75 and 11.5 μs for the $\pi/2$ and π pulses, respectively, at 8 W. The echo delay was equal to 1 rotor period of about 25 μs. Special care was taken with respect to relaxation. Thus, repetition delays of 4 and 15 s for ^1H and ^{19}F NMR, respectively, were found to be long enough for quantitative measurements. For ^{27}Al ($I = 5/2$), the radio frequency field strength of 2.6 kHz was determined from nutation experiments on both cubic solid alum (liquidlike behavior) and berlinite $AlPO_4$ (solid nutation). Selective single-pulse as well as Hahn echo ^{27}Al spectra, with and without ^{19}F high-power decoupling, were collected at a spinning rate of 30 kHz. The single-pulse ^{27}Al MAS NMR spectrum was recorded after excitation with $\pi/12$ pulses and a repetition time of ca. 120 ms. A spin−echo pulse sequence optimized for quadrupolar nuclei was used[37−39] with pulses of 31.5 and 63 μs (nominally a CT selective "solid' 90°−τ−180° sequence for which τ is synchronized to rotor period). High-power efficient decoupling ^{27}Al-{^{19}F} experiments in both the single-pulse and Hahn echo sequences were carried out using the XiX scheme[40] with a decoupling strength of ca. 118 kHz. Simulations of spectra were done with the dmFit[41] software package.

Results and Discussion

Structural Description. The structure of $Al_2F_8 \cdot 2NC_5H_6 \cdot C_6H_3(CO_2H)_3$ consists of a one-dimensional double chain of AlF_6 octahedra intercalated by the pyridine and btc species. There are two crystallographically inequivalent aluminum atoms, Al1 and Al2. Each aluminum atom is coordinated to six fluorine anions (Figure 1) which have different bonding configurations (terminal, corner-bridging, and edge-bridging). Two crystallographically equivalent aluminum atoms have a common edge with Al−F distances of 1.837(1) and 1.887(1) Å for Al1−F1 and 1.853(1) and 1.866(1) Å for Al2−F6. The two distinct pairs of AlF_6 octahedra are linked to each other via corner-sharing with the two fluorine atoms, F2 and F5, located in trans (Al1−F2 = 1.828(1) Å and Al1−F5 = 1.834(1) Å, Al2−F2 = 1.825(1) Å and Al2−F5 = 1.836(1) Å). This generates an infinite straight double chain of $[Al_2F_8]^{2-}$ bioctahedral units running along the *a* axis. Two fluorine atoms are terminal for each aluminum atom, and shorter Al−F distances are expected (Al1−F3 = 1.733(2) Å and Al1−F4 = 1.744(1) Å, Al2−F7 = 1.742(2) Å and Al2−F8 = 1.748(1) Å). The $([Al_2F_8]^{2-})_n$ files are surrounded by protonated pyridine species which occupy two crystallographically inequivalent positions. Both amine molecules interact strongly via hydrogen bonding with one of the terminal fluorine atoms belonging to each distinct aluminum atom through the ammonium groups (N1A−H1A···F3 = 2.062(3) Å and N1B−H1B···F7 = 1.855(2) Å) (Figure 2). The resulting mixed pyridine−fluoroaluminate chains, $([Al_2F_8]^{2-} \cdot [NC_5H_6])_n$, are intercalated by the btc species to make a two-dimensional network of mixed organic−Al_2F_8 moieties in the *bc* plane. Indeed, very strong hydrogen bond interactions are observed between the hydrogen atoms of the protonated carboxylic function and the terminal fluoride anions, F4 and F8, of each aluminum cation (O3−H3···F4

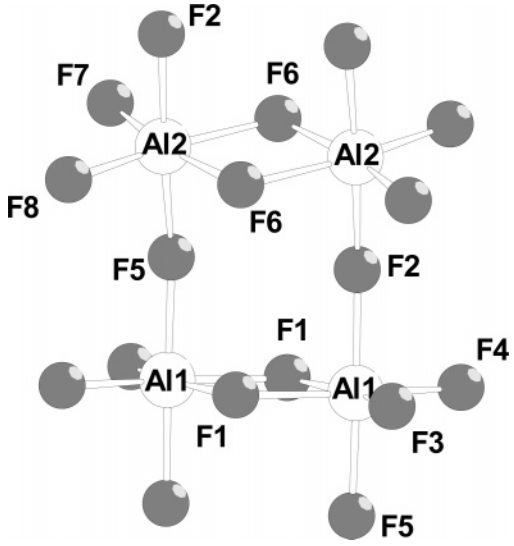

Figure 1. Aluminum−fluorine bond scheme and label atoms of the Al_4F_{18} unit.

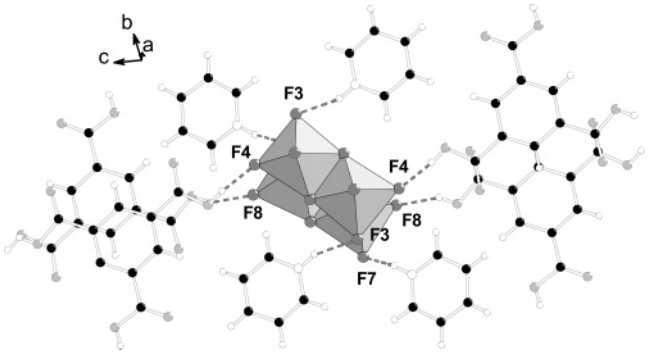

Figure 2. Hydrogen bond interaction of the terminal fluorine of the $([Al_2F_8]^{2-})_n$ chain, the hydrogen atoms of terminal carboxylic acid, and the nitrogen atoms of pyridinium cations.

(37) Man, P. P. *Phys. Rev. B* **1997**, *55*, 8406.
(38) Chan, J. C. C. *Concepts Magn. Reson.* **1999**, *11*, 363.
(39) Stebbins, J. F.; Du, L. S.; Kroeker, S.; Neuhoff, P.; Rice, D.; Frye, J.; Jakobsen, H. J. *Solid State Nucl. Magn. Reson.* **2002**, *21*, 105.
(40) Detken, A.; Hardy, E. H.; Ernst, M.; Meier, B. H. *Chem. Phys. Lett.* **2002**, *356*, 298.
(41) Massiot, D.; Fayon, F.; Capron, M.; King, I.; LeCalve, S.; Alonso, B.; Durand, J. O.; Bujoli, B.; Gan, Z.; Hoatson, G. *Magn. Reson. Chem.* **2002**, *40*, 70.

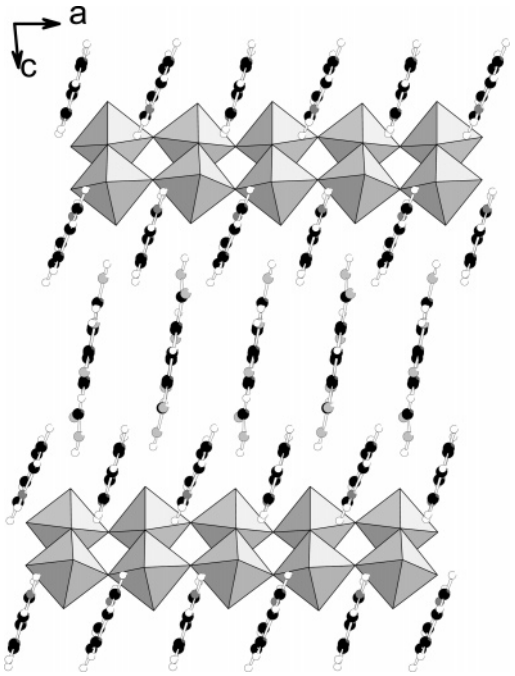

Figure 3. View of the structure of $Al_2F_8{\cdot}2NC_5H_6{\cdot}C_6H_3(CO_2H)_3$ along the *b* axis showing the stacking of pyridine through $\pi-\pi$ interactions and trimesic acid molecules along the *a* axis.

= 1.694(2) Å and O1−H1···F8 = 1.785(2) Å) (Figure 2). Along the *a* axis (Figure 3), the benzene rings of the pyridinium cations are stacked so that strong $\pi-\pi$ interactions occur (C···C ≈ 3.5−3.7 Å). Similar molecular stacking is observed for the btc along the *a* axis, but such $\pi-\pi$ interactions do not exist because of the longer C−C distances (C···C ≈ 4.5 Å). However, there are intermolecular O−H···O hydrogen bonds (O5−H5···O2 = 2.027(2) Å) between the carboxylic acid functions (which are not engaged with F···HO_2C hydrogen bonds) of two adjacent btc molecules along the *b* axis. This type of molecular stacking is common in organic compounds containing aromatic rings; their crystal structures are usually dominated by the $\pi-\pi$ interactions between molecules which generate layered atomic arrangements. We think that the strong stacking character of the pyridine and btc species would favor the formation of a linear chain of inorganic aluminum fluoride and not isolated [AlF_6] clusters. Therefore, the stacking of the benzene-based molecules preferentially in one direction would induce the infinite polymeric condensation of the $(AlF_6)^{3-}$ species for making inorganic chains. This would also be supported by the synthesis conditions of this specific phase which was obtained in a predominantly nonaqueous solvent. Here, pyridine was used as the main solvent, and its anisotropic character (plane geometry) may also reflect a preferential pre-organization of one-dimensional polymeric units in solution. In addition to their stacking features, the two organic molecules play distinct roles: the btc molecules act as linkers between the infinite $([Al_2F_8]^{2-})_n$ files along the *c* axis (via F···HO_2C hydrogen bonding) and are connected to each other along the *b* axis (via COHO···HO_2C hydrogen bonding); this ensures the three-dimensional cohesion of the crystal structure. Pyridine, observed in its protonated form, mainly

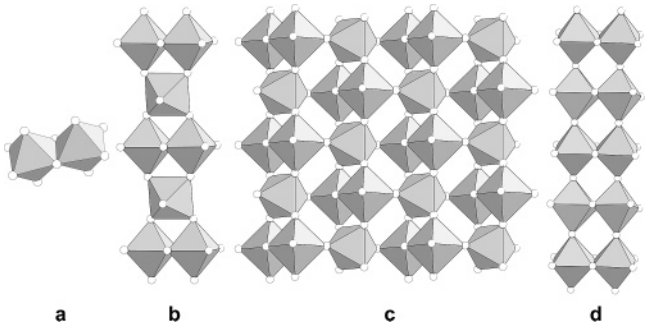

Figure 4. View of the organically templated aluminum fluorides showing the edge-shared connection mode of the AlF_6 octahedra. (a) Isolated bioctahedral species $[Al_2F_{10}]^{4-}$; (b) 1D chain of $[Al_2F_8]^{2-}$; (c) 2D structure of $[Al_3F_{10}]^-$, built up from the connection of infinite type files $[Al_2F_8]^{2-}$; and (d) this work.

interacts with the $([Al_2F_8]^{2-})_n$ chain through the N−H···F hydrogen bond. It would rather act as a compensator for balancing the negative charge of the inorganic file.

The occurrence of an edge-shared octahedral unit is quite rare in the crystal chemistry of metal fluorides, especially in the aluminum-based materials. Usually, only corner-shared octahedra AlF_6 connection modes are observed in the different fluoroaluminates for which various dimensionalities (chain, layer, or 3D network) have been identified. However, a few cases of octahedral motifs with common edges were recently reported. Three phases were obtained exclusively in the presence of cyclic amine (pyridine, piperazine, or 2,4,6-trimethylpyridine) as a countercation (Figure 4). Molecular compounds based on isolated bioctahedral cluster $[Al_2F_{10}]^{4-}$ have been isolated with pyridine[29] (room temperature) and piperazine[30] (185 °C). A similar motif was also reported in the fluoroaluminate salt obtained with tetramethylammonium ions.[28] In the latter, a terminal water belongs to the coordination sphere of aluminum in the molecular $[Al_2F_8(H_2O)_2]^{2-}$ species. The basic bioctahedral building unit is encountered in the chainlike structure of $[Al_2F_8]^{2-}$ synthesized in the presence of 2,4,6-trimethylpyridine[31] at 120 °C. The infinite chain of $[Al_2F_8]^{2-}$ consists of the alternation of bioctahedral motifs $[Al_2F_8]^{2-}$ linked by corner-sharing to each other through an additional octahedral unit AlF_6. The last example was reported by workers from Dupont;[32] they described the synthesis and structure of a layered aluminum fluoride $[Al_3F_{10}]^-$ obtained with pyridine at 275 °C. The two-dimensional network is built up from the corner-shared connection of the $[Al_2F_8]^{2-}$ chain previously identified by Herron et al.[31] Thus, the original connectivity mode observed in our mixed pyridine−carboxylic acid compound constitutes a new possibility for atomic arrangement in aluminum fluorides.

NMR Investigations. In general, hexafluoroaluminate compounds containing isolated regular AlF_6^{3-} octahedra have ^{27}Al peaks in the range between −16 and 1 ppm.[42] Because of the narrow range of chemical shifts[43] as well as the large quadrupole coupling constants, poorly resolved NMR spectra

(42) von Barner, J. H.; Bessada, C.; Berg, R. W. *Inorg. Chem.* **2003**, *42*, 1901.
(43) Yu, P.; Phillips, B. L.; Casey, W. H. *Inorg. Chem.* **2001**, *40*, 4750.

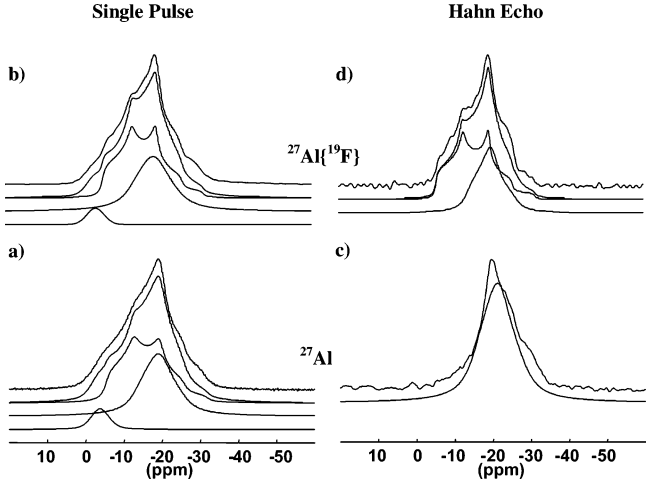

Figure 5. Single-pulse (a) ^{27}Al and (b) ^{27}Al{^{19}F} high-power decoupling and Hahn echo (c) ^{27}Al and (d) ^{27}Al{^{19}F} high-power decoupling NMR spectra of $Al_2F_8{\cdot}2NC_5H_6{\cdot}C_6H_3(CO_2H)_3$. Experimental spectra are presented at the top, while the simulated spectra and its decomposition are shown below. The fits include the central transition pattern line of Al1 and Al2 and the satellite transition of Al2. The latter is present only in the single-pulse experiments.

Table 2. Data of Al Sites Present in $Al_2F_8{\cdot}2NC_5H_6{\cdot}C_6H_3(CO_2H)_3$ Obtained by a Simulation of the ^{27}Al NMR Spectra in Single-Pulse and Hahn Echo Experiments with and without ^{19}F High-Power Decoupling (Figure 5)

NMR experiment	signal	intensity[a]	QCC[b]	η[c]	δ_{iso}[d]
		Single-Pulse			
^{27}Al	Al1	58%	5.5	0.48	−4.3
	Al2	42%	3.4	1.00	−13.4
^{27}Al{^{19}F}	Al1	59%	5.4	0.51	−4.6
	Al2	41%	3.5	1.00	−13.0
		Hahn Echo			
^{27}Al	–	–	–	–	–
	Al2	100%	3.5	1.00	−15.4
^{27}Al{^{19}F}	Al1	59%	5.4	0.48	−4.6
	Al2	41%	3.5	1.00	−13.8

[a] Accuracy: ±1%. [b] Quadrupole coupling constant (QCC) = $(e^2qQ)/h$ with the *z*-component, $V_{zz} = eq$, of the electric field gradient, the electric quadrupole moment, eQ, of ^{27}Al nuclei, and Plank's constant, h. Accuracy: ±0.1 MHz. [c] Asymmetry parameter, $\eta = (V_{xx} - V_{yy})/V_{zz}$, as a function of the *x*, *y*, and *z* components of the electric field gradient. Accuracy: ±0.02. [d] Isotropic chemical shift. Accuracy: ±0.4 ppm.

are usually expected in solid aluminum fluoride. The ^{27}Al MAS NMR spectrum of $Al_2F_8{\cdot}2NC_5H_6{\cdot}C_6H_3(CO_2H)_3$ recorded in single-pulse mode (Figure 5a) agrees with the presence of aluminum exclusively in a coordination number of six.[44] It consists of two broad quadrupolar patterns with different quadrupole coupling constants of 3.5 and 5.4 MHz (see Table 2). The two signals, which have an intensity ratio of almost 1 to 1, are consistent with crystallographic sites Al1 and Al2 in agreement with XRD analysis. The signal with a larger quadrupole coupling constant, which indicates higher distortion of the Al local environment, is assigned to the Al1 site which has a lower regular Al−F distance distribution than the Al2 site (Table 2). Moreover, the hydrogen bond interaction network of the organic molecules with fluorine is less symmetric around Al1 (H···F = 2.062 and 1.694 Å) than it is around Al2 (H···F = 1.855 and 1.785 Å) and is, therefore, consistent with the assignment of Al1 to the signal with a larger quadrupolar coupling constant. A high-power decoupling ^{27}Al{^{19}F} experiment leads to a better resolved spectrum (Figure 5b) by removal of the residual heteronuclear ^{19}F−^{27}Al dipolar interaction not completely averaged by MAS. The increased resolution produces better spectra simulations and confirms the obtained NMR parameters. The result from the ^{27}Al echo MAS NMR spectrum is shown in Figure 5c. In contrast to single-pulse experiments, only the signal for the Al2 site is observed under our experimental conditions. The Al1 signal has a larger quadrupole coupling constant and is undetected, presumably, because of the shorter echo decay in comparison to that of the Al2 signal. Magnetization loss caused by spin diffusion via the strongly coupled S nuclei (^{19}F or ^{1}H) may decrease the phase coherence of the observed spin system (^{27}Al) leading to a collapse of the echo intensity.[45,46] The observation of both Al1 and Al2 signals in a spin−echo MAS experiment under efficient high-power decoupling ^{27}Al{^{19}F} conditions (Figure 5d) strengthens this assumption. However, since both Al sites are chemically very similar, where global Al−F distances in one site are very close to those in the other site, the heteronuclear dipolar interactions alone could not account for the differentiation between the two sites in the two experiments. Therefore, a combination of strong quadrupolar and heteronuclear dipolar interactions probably drives the decay of the signal.

The spectrum of just the central transition centerbands obtained in the selective MAS Hahn echo experiment with ^{19}F high-power decoupling (Figure 5d) can be simulated extremely well by using δ_{iso}, QCC, and η values to simulate the corresponding single-pulse spectrum under the same ^{19}F decoupling conditions (Figure 5b). The values obtained by simulation of the selective Hahn echo ^{27}Al{^{19}F} spectrum are $\delta_{iso} = -4.6$, QCC = 5.4 MHz, and $\eta = 0.48$ for one site and $\delta_{iso} = -13.8$, QCC = 3.5 MHz, and $\eta = 1.00$ for the other site. The only significant difference between the simulated values for the single-pulse and Hahn echo ^{27}Al{^{19}F} spectra is the simulated value of δ_{iso} for the second site ($\delta = 13.0$ vs $\delta = 13.8$). Because the Hahn echo sequence allows the satellite transitions, one of which overlaps with the central transition in the one-pulse spectra, to be completely removed, the simulated Hahn echo spectrum provides the most meaningful values for δ_{iso}, QCC, and η. Table 2 presents our best estimates for δ_{iso}, QCC, and η obtained from ^{27}Al spectra acquired in the different experimental conditions using one-pulse and Hahn echo sequences with and without ^{19}F high-power decoupling.

The ^{19}F MAS NMR spectrum of $Al_2F_8{\cdot}2NC_5H_6{\cdot}C_6H_3(CO_2H)_3$ shows signals with isotropic chemical shift, δ_{iso}, values from −145 to −162 which are in good agreement with typical ^{19}F NMR spectra of various crystalline AlF_3 phases composed of AlF_6 octahedra.[47] Four components at −145.0 (26%), −155.3 (38%), −160 (23%), and −161.9

(44) Robert, E.; Lacassagne, V.; Bessada, C.; Massiot, D.; Gilbert, B.; Coutures, J. P. *Inorg. Chem.* **1999**, *38*, 214.
(45) Haase, J.; Oldfield, E. *J. Magn. Reson. A* **1993**, *101*, 30.
(46) Gee, B. A. *Magn. Reson. Chem.* **2004**, *42*, 30.
(47) Krahl, T.; Stosser, R.; Kemnitz, E.; Scholz, G.; Feist, M.; Silly, G.; Buzare, J. Y. *Inorg. Chem.* **2003**, *42*, 6474.

ppm (13%) are observed and correspond to four distinct F environments in the compound. However, according to XRD data, eight crystallographic fluorine sites (F1−F8) exist within the structure with equal population. The experimental NMR result could be seen as a set of signals with a 2:3:2:1 ratio accounting for the eight crystallographic F atoms. The strong homonuclear dipolar $^{19}F-^{19}F$ interactions as well as the quadrupolar interaction of ^{27}Al indirectly coupled to ^{19}F may hinder a complete spectral resolution of those sites. In view of the lack of resolution, we did not attempt to make assignments.

The ^1H MAS NMR spectrum of $Al_2F_8 \cdot 2NC_5H_6 \cdot C_6H_3(CO_2H)_3$ exhibits at least three signals. The main signal at 8.3 ppm is from the protons in the aromatic ring of the protonated pyridine (Pyr-H^+). The shoulder at 6.7 ppm is assigned to the aromatic protons of btc. The broad peak at 13.4 ppm is assigned to the carboxylic acid group signal (COOH) overlapping with the pyridinium ion signal (Pyr-H^+). The assignment is done on the basis of quantification. Indeed, the experimental NMR intensities of those respective signals are 54%, 23%, and 23% for 8.3, 6.7, and 13.4 ppm, respectively, while the expected corresponding values from the calculations, according to the chemical composition, are 55% for aromatic H in Pyr-H^+, 17% for aromatic H in btc, and 28% for acidic protons in btc and Pyr-H^+. These results confirm that the organic molecules are in their acidic forms. Indeed, a solution NMR of trimesic acid in DMSO-d_6 shows two signals at 8.7 and 13.0 ppm, and that of pyridine in DMSO-d_6 exhibits three signals for aromatic protons at 7.4, 7.8, and 8.6 ppm.

Conclusions

Hydrothermal reaction of aluminum nitrate with btc in pyr/HF produces a new aluminum fluoride compound: $Al_2F_8 \cdot 2NC_5H_6 \cdot C_6H_3(CO_2H)_3$. The structure, solved by means of single-crystal X-ray diffraction, consists of inorganic fluoroaluminate chains intercalated by a network of organic molecules composed of carboxylic acid and protonated pyridine. The inorganic framework contains octahedral AlF_6 species connected through either the corner or the edge in a manner which forms the 1D chains of the bioctahedral unit $[Al_2F_8]^{2-}$. The organic molecules interact strongly with the fluoride framework via hydrogen bonding through the carboxylic acid functions and ammonium groups of pyridinium ions. Multinuclear solid-state NMR characterization agrees quite well with the structural description. The two crystallographic Al sites are resolved in ^{27}Al spectra using a combination of selective Hahn echo MAS sequence and ^{19}F high-power decoupling techniques. ^{19}F MAS NMR showed four unresolved signals because of the strong homonuclear dipolar interaction. Quantitative ^1H MAS NMR is consistent with the presence of organic molecules in protonated form.

Supporting Information Available: Crystallographic data for $Al_2F_8 \cdot 2NC_5H_6 \cdot C_6H_3(CO_2H)_3$ (CIF file) and figures showing the structure along the *a* axis, ^{19}F MAS NMR spectra, and ^1H MAS NMR spectra. This material is available free of charge via the Internet at http://pubs.acs.org.

IC048461Z